MATERIALS SCIENCE

Two-dimensional hybrid perovskites sustaining strong polariton interactions at room temperature

A. Fieramosca[1,2]*, L. Polimeno[1,2,3]*, V. Ardizzone[1,2†], L. De Marco[1†], M. Pugliese[1], V. Maiorano[1], M. De Giorgi[1], L. Dominici[1], G. Gigli[1,2], D. Gerace[1,4], D. Ballarini[1], D. Sanvitto[1,3]

Polaritonic devices exploit the coherent coupling between excitonic and photonic degrees of freedom to perform highly nonlinear operations with low input powers. Most of the current results exploit excitons in epitaxially grown quantum wells and require low-temperature operation, while viable alternatives have yet to be found at room temperature. We show that large single-crystal flakes of two-dimensional layered perovskite are able to sustain strong polariton nonlinearities at room temperature without the need to be embedded in an optical cavity formed by highly reflecting mirrors. In particular, exciton-exciton interaction energies are shown to be spin dependent, remarkably similar to the ones known for inorganic quantum wells at cryogenic temperatures, and more than one order of magnitude larger than alternative room temperature polariton devices reported so far. Because of their easy fabrication, large dipolar oscillator strengths, and strong nonlinearities, these materials pave the way for realization of polariton devices at room temperature.

INTRODUCTION

In efficient communication and computing systems, information carriers are required to both travel long distances without losing coherence and simultaneously interact between them to implement logic functions such as switches or logic gates. Microcavity polaritons, quasiparticles that form in a semiconductor when an elementary excitation field interacts sufficiently strongly with the electromagnetic radiation field, could, in principle, fulfill these requirements and are promising candidates for a new generation of optoelectronic devices. These "dressed" photons exhibit enhanced nonlinearities due to their electronic component (*1*, *2*), allowing many-body effects to be studied in optical systems and appearing as building blocks for integrated photonic circuits and electro-optic applications (*3*, *4*). However, to bring strong nonlinearities and good optical properties to room temperature (RT) is a real challenge. Recently, polariton condensation and superfluidity have been observed at RT in organic semiconductors due to the very large binding energy and oscillator strength of Frenkel excitons (*5*). Nevertheless, interactions among excitons in organic materials are usually at least two orders of magnitude lower than the ones observed for typical Wannier-Mott excitons, and the spin degree of freedom, which is of paramount importance for photonic applications, is quickly averaged out. On the other hand, polaritons in layered transition metal dichalcogenide (TMD) materials have been anticipated as a possible approach to resolving this problem, as recently demonstrated (*6*), showing interactions at least 10 times higher than organic materials. However, these must be in single monolayers to function, are difficult to control, and barely achieve extensions of more than several tens of micrometers. Here, we demonstrate that polariton-polariton interactions at RT in two-dimensional (2D) single-crystal perovskites are as high as those measured at cryogenic temperatures in inorganic semiconductors.

Hybrid organic-inorganic perovskite systems have recently attracted a considerable attention driven by exceptional progress in photovoltaics, photonics, and optoelectronics (*7*–*10*). In particular, 2D perovskites are spontaneous realizations of multiple layered quantum well (QW) heterostructures made of $(PbX_6)2-$ tetrahedral inorganic layers, with X indicating a halide, sandwiched between bilayers of organic cations (see Fig. 1A) (*11*, *12*). The lowest-energy electronic excitations are associated with the inorganic sheet, the organic part acting as a potential barrier (*7*, *8*, *13*, *14*).

These 2D layered structures share strong similarities with multi-QW heterostructures made of epitaxially grown inorganic semiconductors, but they have larger binding energies and display stronger dielectric confinement in the inorganic layers. 2D hybrid perovskites also show enhanced collective effects due to the large number of layers stacked in a single crystal, which is an advantage over TMD monolayers. Strong light-matter coupling has already been observed in $MAPbBr_3$ microwire/nanowire cavities (*15*); in particular, evidence for exciton-polariton condensation has recently been reported in all-inorganic perovskite $CsPbX_3$ nanoplatelets (*16*, *17*) and in spin-coated layered hybrid organic-inorganic perovskite thin films (*18*–*20*). Su *et al.* (*21*) have also shown polariton propagation in a $CsPbBr_3$ microcavity wire over a distance of 60 μm. These results indicate huge room for substantial advancements in realization of low-threshold coherent light sources and polaritonic devices with this kind of hybrid organic-inorganic semiconductor (*22*).

In this study, using single crystal of 2D hybrid perovskites, we were able to directly estimate an exciton-exciton interaction constant as high as 3 μeV μm^2. This value is more than one order of magnitude larger than the alternative RT polariton systems reported thus far and is comparable to the system used in all-optical transistors, switches, and gates currently shown to be operable only at cryogenic temperatures in GaAs-based semiconductors.

It is worth noting the strong recent interest in evaluation of such parameters in GaAs- or InGaAs-based polaritons. One of the main difficulties is estimation of the proper density of polaritons and the exciton reservoir that could lead to very diverse values, sometimes differing by many orders of magnitude (*23*–*25*).

To avoid possible overestimation of the interaction constant, we make sure in this study to deal only with polariton states by using a short resonant pulse excitation (50 fs) and a low repetition rate (10 kHz) to

[1]CNR Nanotec, Institute of Nanotechnology, via Monteroni, 73100 Lecce, Italy. [2]Dipartimento di Matematica e Fisica, Università del Salento, via Arnesano, 73100 Lecce, Italy. [3]INFN Istituto Nazionale di Fisica Nucleare, Sezione di Lecce, 73100 Lecce, Italy. [4]Dipartimento di Fisica, Università degli Studi di Pavia, via Bassi 6, 27100 Pavia, Italy.
*These authors contributed equally to this work.
†Corresponding author. Email: v.ardizzone85@gmail.com (V.A.); luisa.demarco@nanotec.cnr.it (L.D.M.)

avoid the possible effect of dark exciton states persisting longer than the time between pulses. Moreover, we use very conservative quantities to estimate the polariton density. The 2D single-crystal perovskite we use is a large single-crystal flake of high quality to avoid nonradiative losses and grain-to-grain heterogeneity usually present in polycrystalline films.

At RT, we find the exciton oscillator strengths to be much larger than in epitaxial GaAs QWs at cryogenic temperatures and with comparable nonlinearities. Because of the large oscillator strength of the excitons and the very good crystal structure of the flakes, formation of polaritonic bands and strong nonlinearities are observed even when these structures are not embedded in a microcavity comprising highly reflecting mirrors. This finding is an important step toward realization of polaritonic devices working at RT with easy fabrication and minimal processing, avoiding complex heterostructures comprising top and bottom Bragg mirrors and prohibitive ultralow temperature of operation.

RESULTS AND DISCUSSION

We synthesize phenethylammonium lead iodide $(C_6H_5(CH_2)_2NH_3)_2PbI_4$ (PEAI) using an anti-solvent vapor-assisted crystallization method (*26*) and subsequent mechanical exfoliation (*11*). The 2D perovskite single crystals we use are large single-crystal flakes of high quality to avoid nonradiative losses and grain-to-grain heterogeneity usually present in polycrystalline films. In this study, we investigate both PEAI single crystals embedded in an optical cavity formed by two distributed Bragg reflectors (DBRs) acting as bottom/top mirrors and bare single crystals. Figure 1A shows a sketch of a single 2D PEAI crystal grown on a DBR formed by seven $Si0_2/Ti0_2$ pairs. A second DBR also formed by seven $Si0_2/Ti0_2$ pairs is sputtered on the single crystal to give rise to an optical Fabry-Perot cavity, where the PEAI 2D crystal is embedded. The optical response of the sample is measured in transmission geometry, where the excitation is provided by a nonresonant continuous-wave laser or a femtosecond pulsed laser resonant on the low polariton branch (see also the Supplementary Materials).

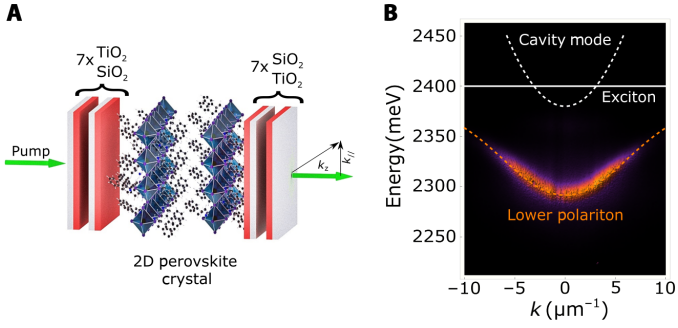

Fig. 1. 2D perovskite single crystal embedded in an optical cavity. (**A**) Schematic representation of a 2D perovskite single crystal embedded in an optical cavity formed by two DBRs; in 2D perovskite, inorganic layers are separated by organic ligands realizing an effective multiple layered QW structure. (**B**) Energy versus in-plane momentum k photoluminescence emission from the sample represented in (A), with $k = \frac{2\pi}{\lambda}\sin\theta$, θ being the emission angle; the white dashed and solid lines represent the cavity and the exciton uncoupled modes, respectively, and the orange line is a fit to the polariton lower mode with E_X = 2.395 eV, E_C = 2.385 eV, and $\hbar\Omega$ = 170 meV.

Figure 1B shows the energy and in-plane momentum-resolved emission from this sample under nonresonant excitation. Because of the strong coupling between the cavity mode and the exciton in the PEAI single crystal, a lower polariton mode is clearly visible with an emission energy of about 2.31 eV at $k = 0$. By fitting the experimental dispersion, we obtain a Rabi splitting $\hbar\Omega$ = 170 meV, with an energy minimum of the cavity mode at E_C = 2.385 eV and an exciton energy E_X = 2.395 eV.

To test the polarization-dependent polariton-polariton interaction in this sample, we measure the resonant transmission of a 50-fs pulsed excitation laser through the sample at normal incidence ($k = 0$). The laser repetition rate is 10 kHz. The large time interval between laser pulses excludes the possibility that the observed dynamics are influenced by reservoir states, which usually have a lifetime no longer than 1 ns. Figure 2A shows the transmission when the laser is linearly polarized, and Fig. 2B shows the transmission when the laser is circularly polarized. Each spectrum in Fig. 2 (A and B) corresponds to different excitation powers, P. As the excitation power increases, we observe a shift of the transmission peak toward higher energies. The energy blueshift of the transmission peaks is plotted in Fig. 2C against the excitation power. As the excitation power increases, we observe a shift of the transmission peak toward higher energies, as expected for a system of interacting particles (*16*, *27*), where the polariton density inside the active medium is proportional to the incident power. Moreover, Fig. 2C shows that the energy blueshift obtained with a circularly polarized laser (blue dots) is higher than the blueshift measured with a linearly polarized laser (red dots). That is, the observed energy blueshift is sensitively larger when all the polaritons are created with the same spin (*28*–*31*). Instead, by using a linear polarized laser (i.e., a coherent superposition of two counter-polarized circular components), only half of the excited polaritons share the same spin, thus roughly halving the interaction

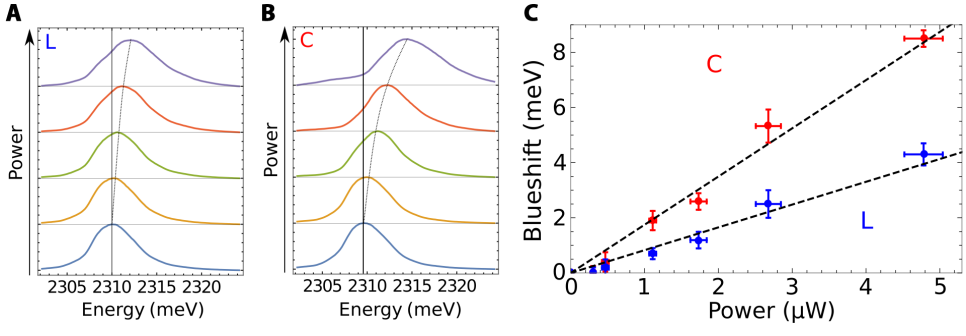

Fig. 2. Nonlinearities in a cavity-embedded perovskite single crystal. (**A**) Transmittivity spectra obtained by cutting the dispersion in Fig. 1B in $k = 0$ and corresponding to different resonant excitation power for linear (A) and circular (**B**) polarized excitation laser. (**C**) Blueshift of the polariton modes in the case of a linear (L) and a circular (C) polarized laser; the dashed lines are linear fit to the experimental data with slopes of 1.75 and 0.83 meV/μW for C and L, respectively.

energy. We notice that the polarization properties of the elementary excitations in these materials arise from the optical transitions connecting the valence band s-type states with total angular momentum quantum numbers ($J = 1/2$, $J_z = \pm 1/2$) to p-type conduction band states with the same symmetry (because of the spin-orbit splitting in the conduction band) (*32*, *33*). Hence, bright exciton states correspond to optical transitions satisfying the condition $\Delta J_z = \pm 1$, which can be excited by using either clockwise or counterclockwise circularly polarized radiation. As a consequence, polariton states are formed with ±1 spin polarization, in close analogy to inorganic semiconductor exciton polaritons in microcavities with embedded QWs.

Thus, the observed spin dependence strongly indicates not only that polariton-polariton interactions are the dominant effect responsible for the energy shift of the modes upon optical excitation but also that 2D perovskites can be used for polariton spintronics. The dashed lines in Fig. 2C are obtained as a linear fit to the experimental points. The ratio between the two slopes is $L/C = 0.47 \pm 0.06$. By following Vladimirova *et al.* (*29*), we can extract the ratio α_2/α_1 from the data of Fig. 2C, in which α_2 is the interaction strength between polaritons with opposite spin and α_1 is the interaction strength between polaritons with the same spin. We then deduce from Fig. 2C a ratio $|\alpha_2/\alpha_1| \sim 0.05$. This value is consistent with the picture of polariton-polariton interactions in standard semiconductors at cryogenic temperature, i.e., a strong repulsive interaction for polaritons with the same spin ($\alpha_1 > 0$) and a weaker interaction for polaritons with opposite spin ($|\alpha_1| \gg |\alpha_2|$). We observe spin-dependent nonlinearities similar to those observed in GaAs-based systems at cryogenic temperatures (*29*).

In the mean-field approximation and at low particle density, the blueshift ΔE_{pol} depends linearly on the polariton density n_{pol}: $\Delta E_{pol} = g_{pol} n_{pol}$. The polariton density n_{pol} is proportional to the excitation power incident on the sample. By analyzing the power dependence of the blueshift, it is possible to measure the polariton interaction constant and then, knowing the polariton excitonic fraction (or Hopfield coefficient), one can finally infer the excitonic interaction constant g_{exc} per layer under circularly polarized excitation. The estimated excitonic interaction constant values for the microcavity sample are $g_{exc} \sim 3 \pm 0.5\,\mu eV\,\mu m^2$. This value is comparable with the one typically estimated for a single GaAs QW (*24*, *25*), and it is the largest measured value at RT so far (see also the Supplementary Materials for details on the calculation of the excitonic interaction constant).

We also note that a small broadening is visible in the spectra of Fig. 2 (A and B) as the incident power increases. This effect can be explained by a time-dependent blueshift given by the exponential decay of the polariton population over time after the passage of the pump pulse. The broadening could result in a small underestimation of g_{exc}. However, we checked its contribution to be negligible, and the spectra of Fig. 2 (A and B) are consistent with the value of the exciton interaction constants obtained by taking the linear blueshift of the peak maxima (*6*). High values of polariton-polariton interaction constants have recently been suggested by numerical simulation of 1D condensate propagation in 3D perovskites (*21*).

The observation of polaritonic nonlinearities at RT in organic-inorganic hybrid materials is a fundamental step to assess their potential for real-world polariton devices. The structure of the sample in Fig. 1A is complex and requires at least a three-step fabrication process: growth of the bottom DBR mirror, growth of the single-crystal flake, and finally growth of the top DBR mirror. Further developments could involve additional fabrication steps like electrical contacts for carrier injection or interconnecting several devices to provide the different functionalities associated with network-on-chip technology. These further steps would result in an even more complex fabrication process, possibly hindering the technological appeal of RT polaritonic devices. However, RT polaritons in 2D single-crystal PEAI flakes have been observed even if the crystal flake is not embedded in an optical cavity formed by highly reflecting mirrors (*32*). Single bare PEAI crystal flakes without cavity are a relatively simpler system to grow. Moreover, the active region can be readily accessed for electrical connections, patterning, or interconnecting several devices. From a technological point of view, assessing RT polariton nonlinearities in single 2D crystals with no cavity is of utmost importance and would lift the complication to embed the perovskite between two mirrors.

Figure 3A shows a sketch of a single 2D PEAI crystal flake grown on a glass substrate. Figure 3B shows in-plane momentum and energy-resolved reflectivity spectra obtained from the single 2D PEAI crystal slab under white light illumination. The optical response of the sample is measured with an oil-immersion microscope objective, which allows us to capture, from the glass substrate side, the signal from the total internal reflection (TIR) at the air-crystal interface (see the Supplementary Materials for details). The measured reflectivity shows a manifold of lower polariton modes (visible as dips in the reflectivity spectra) arising from the coupling of the bare excitonic resonance (white line) with the optical resonances arising from multiple reflections at the top and bottom interfaces of the perovskite slab (*32*). The red dashed lines of Fig. 3B are fits to the lower polariton modes, giving a value of energy coupling between the optical modes and the excitonic transition of $\hbar\Omega \sim 170$ meV. This value is larger than the linewidths of the different resonances involved, and it is thus fully consistent with the strong exciton-photon coupling regime (*32*). In particular, strong coupling between the exciton mode and the optical resonances of the slab is obtained at RT due to the optical confinement given by the refractive index contrast at the interface between the crystal and the surrounding media (air and glass substrate, respectively) and the high value of the excitonic oscillator strength in 2D perovskites.

To understand whether the observed polariton modes of the bare 2D PEAI crystal can sustain nonlinearities at RT, we resonantly excite the single-crystal slab with a femtosecond pulsed laser. The excitation

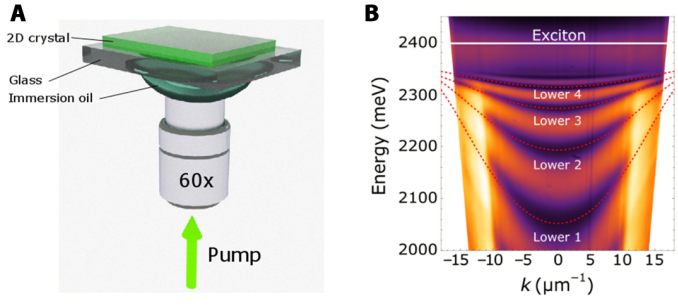

Fig. 3. 2D perovskite single crystal grown on a glass substrate. (**A**) Schematic representation of the TIR configuration adopted for resonant blueshift measurements: An immersion oil objective (60×) is used to focus the excitation beam on a 2D PEAI single-crystal flake grown on a glass substrate; the same objective is used to collect the reflected light. (**B**) Energy and in-plane momentum k resolved reflectivity spectra of a thick single-crystal slab of PEAI; the dips in reflectivity correspond to lower polariton modes resulting from the coupling of the exciton mode to different optical modes; the white line represents the energy of the bare exciton mode; the red dashed lines represent lower polariton modes; the enhanced intensity for $k \geqslant 10\,\mu m^{-1}$ corresponds to angles of incidence beyond the light line between air and the perovskite slab.

beam forms a finite angle with the surface of the slab, corresponding to an in-plane momentum of about $k \sim 12.7\,\mu m^{-1}$. This value of in-plane momentum corresponds to an angle that is beyond the crystal-air TIR angle, which means that all the incident laser power is absorbed or reflected by the sample, where the transmitted part is negligible. The green oval region in Fig. 4A shows the energy and momentum spread of the laser used in resonant excitation. Figure 4B represents a vertical cut of the dispersion of Fig. 4A corresponding to the green region.

This choice of the incident angle, in addition to being in the highest reflectivity region, also allows us to probe polariton modes with a higher excitonic fraction and smaller linewidth. The bandwidth of the femtosecond laser is large enough to resonantly excite essentially three adjacent lower polariton branches. Figure 4B shows that the reflectivity spectra change when the incident power is increased: The low-power resonances (red continuous lines) are shifted at high incident power (blue continuous lines) and then recover their initial energy (red dashed lines) when the incident power is lowered, which guarantees that the blueshift is not due to degradation of the material upon optical excitation. This evidence shows that the observed blueshift arises from interparticle interactions, as observed in low-temperature inorganic polariton systems (*28*–*30*) and in the cavity-embedded single crystal in Fig. 2.

The TIR geometry chosen to perform resonant excitation allows us to neglect the transmission through the sample, simplifying the estimation of the incident power (see also the Supplementary Materials).

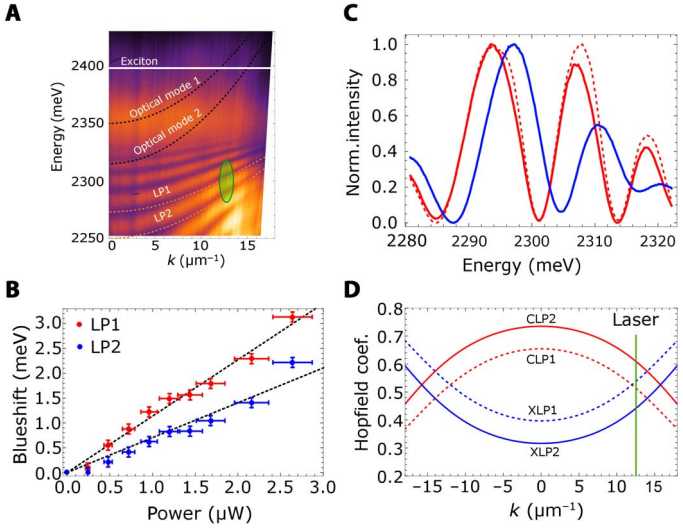

Fig. 4. Nonlinearities in a 2D perovskite single crystal. (**A**) Reflectivity spectra obtained for a PEAI single-crystal slab; the same excitonic mode is coupled to several optical modes of the slab; the two lower polariton modes highlighted by orange dashed lines originate from the coupling of the two optical modes (black dashed lines) to the excitonic mode (white solid line). (**B**) Energy shift of the lower polariton modes of (A) as a function of the incident power; the energy shift is measured at $k \sim 12.7\,\mu m^{-1}$ corresponding to the green region of (A). (**C**) Reversibility of the observed blueshift of the polariton modes; the red continuous curve corresponds to the energy of the polariton modes for low excitation power $P = 10\,\mu J/cm^2$; the continuous blue curve shows the blueshifted modes at high excitation power $P = 150\,\mu J/cm^2$; when the excitation power is reduced, the polariton modes recover the original energy (dashed red curve). (**D**) Hopfield coefficients showing the exciton (XLP1, XLP2) and photon (CLP1, CLP2) fraction of the two lower polariton modes of (A); the green vertical line represents the in-plane momentum of the resonantly created polariton, where LP1 has a larger exciton fraction than LP2.

The two lower polariton branches fitted by the dashed orange lines (LP1 and LP2) originate from the two optical modes highlighted by the two black dashed lines. Polariton modes originating from different cavity modes and coupled to the same excitonic transition have a different excitonic fraction at a given excitation angle. Figure 4C shows the blueshift measured for the lower polariton branches LP1 and LP2 in Fig. 4A as a function of the polariton density by using a linearly polarized pulsed laser. We observe that, for a given incident power (i.e., a given polariton density), the measured blueshift is higher for the polariton branch with the higher excitonic fraction, LP1, which confirms that the energy blueshift increases as the excitonic component increases. By fitting the data in Fig. 4C with a straight line and considering the relation between ΔE_{pol} and n_{pol}, we can obtain the excitonic interaction constant per layer $g_{exc,L}$ under linearly polarized excitation. Given the incident power values and considering that all the absorbed light is transformed into polaritons (which is a very conservative approximation, see the Supplementary Materials), the upper density limit for the exciton density per layer is about $n_{exc,layer} = 10^{12}\ cm^{-2}$. Accounting for the different excitonic fraction of the two lower polariton branches, we obtain a value of the excitonic interaction constant $g_{exc,L} \sim 1 \pm 0.2\,\mu eV\,\mu m^2$ per inorganic layer. This value is comparable with that obtained for the 2D single crystal embedded in a microcavity, as shown in Figs. 1 and 2. In both cases, we used a pulsed resonant laser to estimate the interaction constants, thus avoiding the effects of the polariton-reservoir interactions that would contribute to the blueshift observed and would forbid a direct probe of the polariton-polariton interaction constants. Moreover, we would like to stress that by neglecting any loss in the material, we overestimate the number of excitons in the system; therefore, much larger interaction strengths should be expected, and the reported value of g_{exc} should be taken as a lower bound. Nevertheless, this lower bound is already at least two orders of magnitude higher than typical interaction constants of organic excitons at RT (*34*) and about 20 times larger than the values recently measured in a WS_2 monolayer (*6*).

In summary, we have observed highly interacting polaritons in hybrid organic-inorganic 2D perovskite single crystals at RT. These materials spontaneously crystallize in a multiple layered QW-like structure, and because of the high oscillator strength of the excitonic transition, strong coupling is achieved at RT even without highly reflecting mirrors. The resulting polaritons are highly interacting with an excitonic interaction constant $g_{exc} \sim 3 \pm 0.5\,\mu eV\,\mu m^2$. This value is two orders of magnitude higher than the values measured for organic excitons, and it is the highest measured at RT so far. Moreover, we observe that polariton-polariton interactions in our sample are spin dependent, where the repulsive interaction between polaritons with the same spin is the dominant effect. These results demonstrate that 2D hybrid organic-inorganic perovskites sustain highly interacting polaritons working with interaction constants, which are very promising for future polaritonic and spintronic devices at RT. We observe highly interacting polaritons at RT without embedding the active medium in an optical cavity. These findings are extremely important and promise to greatly reduce the cost and the complexity of fabrication and post-processing of polaritonic devices.

METHODS

Synthesis of 2D perovskite flakes

PEAI solutions were prepared by dissolving equimolar amounts of PbI_2 and phenethylammonium iodide in γ-butyrolactone and

stirring at 70°C for 1 hour. 2D perovskite single crystals were synthesized using an anti-solvent vapor-assisted crystallization method as follows: 5 µl of the perovskite solution was deposited on a glass cover slip and then covered by a second cover slip. Next, a small vial containing 2 ml of dichloromethane was placed on the top of the two sandwiched substrates. Substrates and vial were placed in a larger Teflon vial, closed with a screw cap, and left undisturbed for some hours. After this time, millimeter-sized crystals, with thicknesses varying from few to tens of micrometers, appeared in between the two substrates. Single crystals were mechanically exfoliated with the SPV 224PR-M Nitto Tape and transferred onto glass substrates. The exfoliated flakes, with thicknesses of tens of nanometers, appeared smooth and uniform over tens of square micrometers, as observed by scanning electron microscopy and atomic force microscopy.

SUPPLEMENTARY MATERIALS

Supplementary material for this article is available at http://advances.sciencemag.org/cgi/content/full/5/5/eaav9967/DC1

Section S1. Material synthesis
Section S2. Microcavity fabrication
Section S3. Absorption and photoluminescence
Section S4. Optical setup
Section S5. Interaction constant
Fig. S1. Absorption (blue) and photoluminescence (green) spectra measured on top of a PEAI single crystal with a 488-nm continuous-wave laser.
Fig. S2. Optical setup used to measure the microcavity sample.
Fig. S3. Exciton blueshift as a function of exciton density per QW obtained with a linearly polarized laser.
Fig. S4. Microcavity-embedded single crystal.

REFERENCES AND NOTES

1. P. G. Savvidis, J. J. Baumberg, R. M. Stevenson, M. S. Skolnick, D. M. Whittaker, J. S. Roberts, Angle-resonant stimulated polariton amplifier. *Phys. Rev. Lett.* **84**, 1547–1550 (2000).
2. C. Weisbuch, M. Nishioka, A. Ishikawa, Y. Arakawa, Observation of the coupled exciton-photon mode splitting in a semiconductor quantum microcavity. *Phys. Rev. Lett.* **69**, 3314–3317 (1992).
3. I. Carusotto, C. Ciuti, Quantum fluids of light. *Rev. Mod. Phys.* **85**, 299–366 (2013).
4. D. Sanvitto, S. Kéna-Cohen, The road towards polaritonic devices. *Nat. Mater.* **15**, 1061–1073 (2016).
5. G. Lerario, A. Fieramosca, F. Barachati, D. Ballarini, K. S. Daskalakis, L. Dominici, M. De Giorgi, S. A. Maier, G. Gigli, S. Kéna-Cohen, D. Sanvitto, Room-temperature superfluidity in a polariton condensate. *Nat. Phys.* **13**, 837–841 (2017).
6. F. Barachati, A. Fieramosca, S. Hafezian, J. Gu, B. Chakraborty, D. Ballarini, L. Martinu, V. Menon, D. Sanvitto, S. Kéna-Cohen, Interacting polariton fluids in a monolayer of tungsten disulfide. *Nat. Nanotechnol.* **13**, 906–909 (2018).
7. L. Pedesseau, D. Sapori, B. Traore, R. Robles, H.-H. Fang, M. A. Loi, H. Tsai, W. Nie, J.-C. Blancon, A. Neukirch, S. Tretiak, A. D. Mohite, C. Katan, J. Even, M. Kepenekian, Advances and promises of layered halide hybrid perovskite semiconductors. *ACS Nano* **10**, 9776–9786 (2016).
8. B. Saparov, D. B. Mitzi, Organic–inorganic perovskites: Structural versatility for functional materials design. *Chem. Rev.* **116**, 4558–4596 (2016).
9. B. R. Sutherland, E. H. Sargent, Perovskite photonic sources. *Nat. Photon.* **10**, 295–302 (2016).
10. F. Thouin, S. Neutzner, D. Cortecchia, V. A. Dragomir, C. Soci, T. Salim, Y. M. Lam, R. Leonelli, A. Petrozza, A. R. S. Kandada, C. Silva, Stable biexcitons in two-dimensional metal-halide perovskites with strong dynamic lattice disorder. *Phys. Rev. Mater.* **2**, 034001 (2018).
11. W. Niu, A. Eiden, G. V. Prakash, J. J. Baumberg, Exfoliation of self-assembled 2D organic-inorganic perovskite semiconductors. *Appl. Phys. Lett.* **104**, 171111 (2014).
12. O. Yaffe, A. Chernikov, Z. M. Norman, Y. Zhong, A. Velauthapillai, A. van der Zande, J. S. Owen, T. F. Heinz, Excitons in ultrathin organic-inorganic perovskite crystals. *Phys. Rev. B* **92**, 045414 (2015).
13. T. Ishihara, J. Takahashi, T. Goto, Optical properties due to electronic transitions in two-dimensional semiconductors $(C_nH_{2n+1}NH_3)_2PbI_4$. *Phys. Rev. B* **42**, 11099–11107 (1990).
14. T. Kondo, S. Iwamoto, S. Hayase, K. Tanaka, J. Ishi, M. Mizuno, K. Ema, R. Ito, Resonant third-order optical nonlinearity in the layered perovskite-type material $(C_6H_{13}NH_3)_2PbI_4$. *Solid State Commun.* **105**, 503–506 (1998).
15. S. Zhang, Q. Shang, W. Du, J. Shi, Z. Wu, Y. Mi, J. Chen, F. Liu, Y. Li, M. Liu, Q. Zhang, X. Liu, Strong exciton-photon coupling in hybrid inorganic-organic perovskite micro/nanowires. *Adv. Optic. Mater.* **6**, 1701032 (2018).
16. R. Su, C. Diederichs, J. Wang, T. C. H. Liew, J. Zhao, S. Liu, W. Xu, Z. Chen, Q. Xiong, Room-temperature polariton lasing in all-inorganic perovskite nanoplatelets. *Nano Lett.* **17**, 3982–3988 (2017).
17. K. Park, J. W. Lee, J. D. Kim, N. S. Han, D. M. Jang, S. Jeong, J. Park, J. K. Song, Light matter interactions in cesium lead halide perovskite nanowire lasers. *J. Phys. Chem. Lett.* **7**, 3703–3710 (2016).
18. T. Fujita, Y. Sato, T. Kuitani, T. Ishihara, Tunable polariton absorption of distributed feedback microcavities at room temperature. *Phys. Rev. B* **57**, 12428–12434 (1998).
19. K. Pradeesh, J. J. Baumberg, G. V. Prakash, Strong exciton-photon coupling in inorganic-organic multiple quantum wells embedded low-Q microcavity. *Opt. Express* **17**, 22171–22178 (2009).
20. A. Brehier, R. Parashkov, J. S. Lauret, E. Deleporte, Strong exciton-photon coupling in a microcavity containing layered perovskite semiconductors. *Appl. Phys. Lett.* **89**, 171110 (2006).
21. R. Su, J. Wang, J. Zhao, J. Xing, W. Zhao, C. Diederichs, T. C. H. Liew, Q. Xiong, Room temperature long-range coherent exciton polariton condensate flow in lead halide perovskites. *Sci. Adv.* **4**, eaau0244 (2018).
22. T. Low, A. Chaves, J. D. Caldwell, A. Kumar, N. X. Fang, P. Avouris, T. F. Heinz, F. Guinea, L. Martin-Moreno, F. Koppens, Polaritons in layered two-dimensional materials. *Nat. Mater.* **16**, 182–194 (2017).
23. Y. Sun, Y. Yoon, M. Steger, G. Liu, L. N. Pfeier, K. West, D. W. Snoke, K. A. Nelson, Direct measurement of polariton–polariton interaction strength. *Nat. Phys.* **13**, 870–875 (2017).
24. P. M. Walker, L. Tinkler, D. V. Skryabin, A. Yulin, B. Royall, I. Farrer, D. A. Ritchie, M. S. Skolnick, D. N. Krizhanovskii, Ultra-low-power hybrid light–matter solitons. *Nat. Commun.* **6**, 8317 (2015).
25. P. M. Walker, L. Tinkler, B. Royall, D. V. Skryabin, I. Farrer, D. A. Ritchie, M. S. Skolnick, D. N. Krizhanovskii, Dark solitons in high velocity waveguide polariton fluids. *Phys. Rev. Lett.* **119**, 097403 (2017).
26. F. Lédée, G. Trippé-Allard, H. Diab, P. Audebert, D. Garrot, J.-S. Lauret, E. Deleporte, Fast growth of monocrystalline thin films of 2d layered hybrid perovskite. *CrystEngComm* **19**, 2598–2602 (2017).
27. M. Wouters, I. Carusotto, Excitations in a nonequilibrium Bose-Einstein condensate of exciton polaritons. *Phys. Rev. Lett.* **99**, 140402 (2007).
28. C. Ciuti, P. Schwendimann, B. Deveaud, A. Quattropani, Theory of the angle-resonant polariton amplifier. *Phys. Rev. B* **62**, R4825–R4828 (2000).
29. M. Vladimirova, S. Cronenberger, D. Scalbert, K. V. Kavokin, A. Miard, A. Lemaître, J. Bloch, D. Solnyshkov, G. Malpuech, A. V. Kavokin, Polariton-polariton interaction constants in microcavities. *Phys. Rev. B* **82**, 075301 (2010).
30. M. Vladimirova, S. Cronenberger, D. Scalbert, M. Nawrocki, A. V. Kavokin, A. Miard, A. Lemaître, J. Bloch, Polarization controlled nonlinear transmission of light through semiconductor microcavities. *Phys. Rev. B* **79**, 115325 (2009).
31. D. Ballarini, A. Amo, L. Viña, D. Sanvitto, M. S. Skolnick, J. S. Roberts, Transition from the strong- to the weak-coupling regime in semiconductor microcavities: Polarization dependence. *Appl. Phys. Lett.* **90**, 201905 (2007).
32. A. Fieramosca, L. De Marco, M. Passoni, L. Polimeno, A. Rizzo, B. L. T. Rosa, G. Cruciani, L. Dominici, M. De Giorgi, G. Gigli, L. C. Andreani, D. Gerace, D. Ballarini, D. Sanvitto, Tunable out-of-plane excitons in 2D single-crystal perovskites. *ACS Photonics* **5**, 4179–4185 (2018).
33. D. Giovanni, W. K. Chong, H. A. Dewi, K. Thirumal, I. Neogi, R. Ramesh, S. Mhaisalkar, N. Mathews, T. C. Sum, Tunable room-temperature spin-selective optical stark effect in solution-processed layered halide perovskites. *Sci. Adv.* **2**, e1600477 (2016).
34. K. S. Daskalakis, S. A. Maier, R. Murray, S. Kéna-Cohen, Nonlinear interactions in an organic polariton condensate. *Nat. Mater.* **13**, 271–278 (2014).

Acknowledgments: We thank P. Cazzato for technical support. **Funding:** We acknowledge the ERC project ElecOpteR (grant number 780757) and the project "TECNOMED—Tecnopolo di Nanotecnologia e Fotonica per la Medicina di Precisione" [Ministry of University and Scientific Research (MIUR) Decreto Direttoriale n. 3449 del 4/12/2017, CUP B83B17000010001]. G.G. acknowledges the project PERSEO-PERrovskite–based Solar cells: towards high

Efficiency and lOng-term stability (Bando PRIN 2015-Italian MIUR Decreto Direttoriale 4 novembre 2015 n. 2488, project number 20155LECAJ). **Author contributions:** A.F. and L.P. performed the optical measurements. A.F., L.P., M.P., and L.D.M. prepared the materials and samples. V.A., L.D.M., L.D., M.D.G., and V.M. contributed to the experimental realization and interpretation of the results. V.A. and L.D.M. wrote the paper with input from all authors. L.D.M., D.G., D.B., V.M., G.G., and D.S. supervised the work. **Competing interests:** The authors declare that they have no competing interests. **Data and materials availability:** All data needed to evaluate the conclusions in the paper are present in the paper and/or the Supplementary Materials. Additional data related to this paper may be requested from the authors.

Submitted 8 November 2018
Accepted 25 April 2019
Published 31 May 2019
10.1126/sciadv.aav9967

Citation: A. Fieramosca, L. Polimeno, V. Ardizzone, L. De Marco, M. Pugliese, V. Maiorano, M. De Giorgi, L. Dominici, G. Gigli, D. Gerace, D. Ballarini, D. Sanvitto, Two-dimensional hybrid perovskites sustaining strong polariton interactions at room temperature. *Sci. Adv.* **5**, eaav9967 (2019).